AMERICAN JOURNAL OF PHYSIOLOGY

ENDOCRINOLOGY AND METABOLISM.

RESEARCH ARTICLE

Alpha cells transdifferentiate into delta cells during the progression of autoimmunity in nondiabetic NOD mice

Zhehui Li,[1] Xinyun Wu,[1] Qi Kang,[1] Qi Ren,[1] Yi Zhang,[1] Yi Zhang,[2] Quanwen Jin,[1] F. Susan Wong,[3] and Mingyu Li[1,4]

[1]*State Key Laboratory of Cellular Stress Biology and Fujian Provincial Key Laboratory of Innovative Drug Target Research, School of Pharmaceutical Sciences and School of Life Sciences, Xiamen University, Xiamen, People's Republic of China;* [2]*Department of Endocrinology, Quanzhou First Hospital Affiliated to Fujian Medical University, Quanzhou, People's Republic of China;* [3]*Division of Infection and Immunity, Cardiff University School of Medicine, Cardiff, United Kingdom;* and [4]*State Key Laboratory of Vaccines for Infectious Diseases,Xiang An Biomedicine Laboratory, Xiamen University, Xiamen, People's Republic of China*

Abstract

The incidence of type 1 diabetes (T1D) has increased in recent years. Although extensive research has focused on immune damage to insulin-producing beta cells, the pathophysiological effects on other endocrine cells within pancreatic islets remain less well-documented. This study investigates the changes in the number and proportion of alpha, beta, and delta cells, as well as hormone secretion, during the progression of autoimmunity in nondiabetic nonobese diabetic (NOD) mice at different ages. Our findings reveal significant heterogeneity in islet size, endocrine cell composition, and degree of immune infiltration. We propose a novel classification system for islet subtypes based on this observed heterogeneity. Notably, we noticed an age-related increase in delta cells in older nondiabetic NOD mice. In addition, we observed an increase in glucagon and somatostatin double-positive cells following immune cell infiltration in nondiabetic mice. Our further analysis demonstrated that these double-positive cells represent a transdifferentiation process from alpha cells to delta cells, mediated by an alpha cell dedifferentiation intermediate. Moreover, our results indicated that the increased presence of delta cells and somatostatin in pancreatic islets significantly inhibits alpha cell function during the progression of autoimmunity. Thus, our findings provide valuable insights into the dynamic changes in alpha and delta cells throughout the natural history of T1D.

NEW & NOTEWORTHY The NOD mouse is widely used as an T1D animal model. Although the mice have the same genetic background, approximately 20% of female NOD mice do not develop diabetes. In this study, we reveal that alpha cells dedifferentiate and then transdifferentiate into delta cells during the progression of autoimmunity in nondiabetic NOD mice. The increased delta cells secrete more somatostatin, which inhibits alpha cell secretion of glucagon, thereby potentially attenuating the increase in blood glucose levels in these mice.

alpha cell transdifferentiation; delta cells; islet heterogeneity; NOD mice; type 1 diabetes

INTRODUCTION

Type 1 diabetes (T1D) is an autoimmune disorder characterized by the immune-mediated destruction of pancreatic beta cells, resulting in reduced insulin secretion (1). To date, T1D treatment has predominantly centered on insulin therapy, with numerous studies focusing on beta cell dysfunction. In addition to insufficient insulin production, elevated circulating glucagon levels have been observed both postprandially and at rest in individuals with T1D (2–4). However, a subset of individuals with T1D experience severe hypoglycemia following insulin administration due to impaired glucagon responses (5). These observations suggest that both insulin deficiency and dysregulation of glucagon release and function contribute to the pathophysiology of T1D. Although several studies have reported changes in alpha cells in nonobese diabetic (NOD) mice, the findings regarding changes in alpha cell mass remain controversial. Pechhold et al. (6) observed a decrease in alpha cell mass in diabetic NOD mice, whereas others have noted an increase (7, 8). These discrepancies may arise from differences in the timepoints chosen for observation.

Regarding delta cells in NOD mice, both the proportion and mass of delta cells increase during T1D progression (7, 9). This increase has also been observed in individuals with T1D (10). Moreover, one previous study has documented an ~30% increase in fasting circulating somatostatin levels in individuals with T1D (11). In addition, delta cells secrete

more somatostatin in inflammatory environments, and in the absence of beta cells, inhibit alpha cell glucagon secretion (12). Thus, although less frequently addressed in previous studies, delta cells may play a significant functional role in T1D. However, the underlying mechanisms driving this delta cell expansion remain unclear.

The nonobese diabetic (NOD) mouse, known for spontaneously developing T1D, is widely used as an animal model of T1D (13, 14). Female NOD mice begin exhibiting symptoms of diabetes as early as 12 wk of age, with increasing incidence of hyperglycemia and T1D as they age, reaching a lifetime incidence of ∼80% (15). However, ∼20% of female NOD mice do not develop hyperglycemia before 35 wk of age and are unlikely to progress to diabetes, exhibiting distinct islet characteristics compared with other mice (16).

To gain a more comprehensive understanding of the dynamic changes in alpha and delta cells during autoimmunity progression and the potential mechanisms driving these changes in nondiabetic NOD mice, we conducted a quantitative analysis of alpha, beta, and delta cells in the islets of nondiabetic NOD mice across six age groups (5 to 32 wk). Our results indicate that alpha cell mass remains relatively stable, whereas delta cell mass increases during autoimmunity progression. Furthermore, alpha-to-delta cell transdifferentiation appears to be the primary driver of delta cell expansion in nondiabetic NOD mice. These newly increased delta cells, in turn, inhibit the response of alpha cells to hypoglycemic stimuli.

MATERIALS AND METHODS

Mice

NOD mice were bred and maintained at the Xiamen University Experimental Animal Center. The animals were housed in individually ventilated cages (≤5 mice per cage) within a specific pathogen-free facility with a 12-hour light-dark cycle at a temperature of 20–23°C. They were provided with standard chow and water ad libitum. By 32 wk of age, the cumulative incidence of autoimmune diabetes in our female NOD mice reaches 81% (Supplemental Fig. S1). All experimental procedures were approved by the Animal Care and Use Committee of Xiamen University (Protocol No. XMULAC20220141).

Blood Glucose Monitoring

Female NOD mice were monitored weekly for glycosuria from 8 wk of age. Upon detection of positive glycosuria using a blood glucose meter (Yuwell, China), diabetes was diagnosed when blood glucose levels exceeded 13.9 mmol/L (1), confirmed by a second measurement. Diabetic mice were euthanized via cervical dislocation on the same day of diagnosis, and pancreatic tissue samples were collected. The incidence of diabetes in our NOD mouse colony is illustrated in Supplemental Fig. S1.

Pancreatic Histological Preparation and Immunofluorescence Staining

Whole pancreata were fixed in 4% paraformaldehyde. After infusion with 10% and 20% sucrose at 4°C, the tissues were embedded in optimal cutting temperature (OCT) compound, snap-frozen, and stored at −80°C as previously described (17). Frozen sections were processed according to a standard protocol (18). In brief, 6-µm thick sections were incubated with primary antibodies overnight at 4°C, followed by incubation with secondary antibody for 2 h at room temperature (RT). Images were captured using a Leica SP8 confocal microscope (Leica, Germany), and quantification was performed using ImageJ software (National Institutes of Health). Confocal images were first converted to 8-bit format and split into individual color channels. For each channel, thresholds were set using the "Auto Threshold" function to minimize background and normalize signal intensity across samples. Colocalization was assessed using the "Image Calculator" function with the "AND" operation to generate a mask of overlapping signals. Cells exhibiting overlapping signals for both glucagon and somatostatin were defined as alpha delta double-positive cells.

Primary antibodies used included guinea pig anti-insulin (DAKO, A0564), rabbit anti-glucagon (Abcam, ab92517), mouse anti-glucagon (Sigma-Aldrich, G2654), rat anti-somatostatin (Abcam, ab30788), rat anti-somatostatin (Thermo Fisher Scientific, MA5-16987), mouse anti-CD45 (Abcam, ab33923), mouse anti-neurogenin3 (BD Biosciences, 610790), mouse anti-neurogenin3 (Santa Cruz Biotechnology, Sc-374442), mouse anti-Sox9 (Proteintech Group, 67439-1-Ig), rabbit anti-Aldh1a3 (Novus Biologicals, NBP2-15339), rabbit anti-Nkx6.1 (Abcam, ab221549), and rabbit anti-Ki67 (Abcam, Ab15580).

Pancreatic Islet Isolation

The isolation of islet was performed as previously described (19). Following euthanasia of mice, a buffer containing 1 mg/mL type IV collagenase (Gibco, 17104019) was injected into the common bile duct. The pancreata were dissected and incubated in a 37°C water bath for 10 min, then gently shaken for ∼5 min until complete digestion. The tissue was resuspended, and islets were purified by density gradient centrifugation (Sigma, 10771). Individual islets were handpicked under a dissecting microscope and cultured in 4 mL RPMI 1640 medium (Gibco, C11875500) containing 10% FBS and 1% penicillin/streptomycin in a 37°C incubator. The purity of islet was assessed by dithizone solution, and the isolated islets with purity up than 90% were used for experiments (Supplemental Fig. S2).

Measurement of Islet Hormone Content

Islets from three mice of each age group were pooled. Five islets from each group were randomly selected and placed in 1.5-mL centrifuge tubes. Pre-prepared acidified ethanol (50 mL of 75% ethanol with 750 µL of concentrated hydrochloric acid) was added to each tube. Islets were homogenized and slowly shaken overnight at 4°C. Samples were then centrifuged at 4,000 rpm for 30 min at 4°C, and the supernatant was collected and diluted 100–500 times for measurement of insulin, glucagon, and somatostatin by ELISA (Meimian, China) according to the manufacturer's instructions.

Measurement of Islet Hormone Secretion

Islets from three nondiabetic NOD mice in each age group were pooled and 20 islets from each group were randomly selected and cultured in 96-well plates either with or without the somatostatin receptor 2 inhibitor, 10 nM DOTA-JR11, in

RPMI 1640 medium. Hormone content in the supernatant was measured after culture for 2 and 24 h, respectively.

Calcium Imaging and Quantification of Cytosolic Ca^{2+} Content

Islets from each group were incubated with 5 μM Fluo-4 AM (Invitrogen, F14201) for 1 h in Krebs-Ringer Bicarbonate Buffer (KRBH) solution, supplemented with 6 mM glucose and 0.1% BSA, at 37°C in the dark. The islets were then transferred to a buffer solution containing 20 mM glucose and incubated at 37°C in the dark for 30 min before being plated in an imaging chamber for confocal microscopy on a Leica SP8 system. Time series images were acquired every 10 s (XYZT imaging, stack of 10 confocal images). Alpha cells were identified by their response to stimulation with 10 μM adrenaline. To visualize intracellular Ca^{2+} fluctuations, the average Fluo-4 AM fluorescence intensity per frame was measured using Leica Application Suite X (V2.0.1). Fluorescence intensity was displayed as the ratio of the original fluorescence intensity (F) to the initial fluorescence intensity value (F0) (F/F0). The baseline (F0) of each group was defined as the average fluorescence intensity before stimulation with 1 mM glucose.

DOTA-JR11 Injection and Tail-Tip Blood Sampling

DOTA-JR11 (SSTR2-antagonist) was freshly prepared in sterile saline under light-protected conditions and administered via intraperitoneal injection (100 μL, 10 mg/kg) to five 18-wk-old non-diabetic female NOD mice. Another five age- and cage-matched non-diabetic female NOD mice received an equal volume of sterile saline. Three hours post-injection, all mice were fasted. Starting from the time of intraperitoneal injection, tail-tip blood samples were collected every 6 h thereafter. Blood volume collected at each time point did not exceed 30 μL. Part of the blood was immediately used for glucose measurement, whereas the remaining serum was collected and stored at −80°C for subsequent glucagon analysis.

Single-Cell Sequencing Data Analysis

We utilized published single-cell sequencing data from GSE117770 (20), which reported single-cell sequencing of 8-, 14-, and 16-wk-old nondiabetic NOD mice. The detail information about the single-cell sequencing, including sequencing platform, read depth, cell numbers per sample, mouse strain (pure NOD), and original data processing pipelines, are described in the original publication (20). We reanalyzed these single-cell sequencing data, the quality filtering was performed using multiple filtering criteria including excluding cells with 25% of mitochondrial gene expression, cells fewer than 200 genes expressed, or cells with more than 8,000 genes expressed. Remaining cells were normalized using the NormalizeData function with the LogNormalize method, and highly variable genes were identified using FindVariableFeatures. Unsupervised analysis was carried out using principal component analysis (PCA) via the RunPCA function to identify principal components.The top principal components (PCs) were used for cell clustering. Cells with similar transcriptome profiles were clustered into 26 cell clusters corresponding to 10 cell types, including beta cells, alpha cells, delta cells, PP cells, acinar cells, endothelial cells, immune cells, fibroblasts, smooth muscle cells, and erythroid-like cells. These cells were used for subsequent analysis. Pseudotime analysis was performed using the Monocle2 package (21).

Algorithm for Pancreatic Islet Clustering Based on Size, Infiltration, and Endocrine Cell Proportion

All pancreatic islets were sequentially numbered and labeled with information on their origin (mouse ID), age, health status at the time of death, islet size, number of infiltrating immune cells, and proportion of three types of endocrine cells. Normalization was performed using the NormalizeData function, and feature variables were identified through FindVariableFeatures. Principal components were determined using RunPCA, and clustering was based on these results. The top principal components were used as input for uniform manifold approximation and projection (UMAP) analysis to determine the overall relationship between islets.

Statistical Analysis

Raw data were analyzed with GraphPad Prism 9 software (GraphPad Software, La Jolla, CA; RRID: SCR_002798). Data are presented as means ± SE. No outlying values were excluded from the datasets used for statistical analysis. Two-way ANOVA followed by Bonferroni's post hoc tests was used for two-factor assays. For single-factor assays, unpaired t tests or one-way ANOVA were used. All data were first subjected to the Shapiro–Wilk normality test. If the data followed a Gaussian distribution, parametric tests were performed, followed by Bonferroni's post hoc tests for three or more groups. If the data did not follow a Gaussian distribution, nonparametric tests (Mann–Whitney test for two groups or Kruskal–Wallis test with Dunn's post hoc test for three or more groups) were performed. Differences were considered to be statistically significant when $P < 0.05$.

RESULTS

Dynamic Analysis of Endocrine Cells Reveals an Increase of Delta Cells in Nondiabetic NOD Mice

We examined the pancreas of non-diabetic female NOD mice across six age groups: 5–9 wk, 10–14 wk, 15–19 wk, 20–24 wk, 25–30 wk, and >30 wk (31–32 wk old). Immunofluorescence analysis was carried out on islets from 66 individual female nondiabetic NOD mice at different ages to quantify the number and proportion of alpha, beta, and delta cells, as well as immune cells (Fig. 1A). As shown in Fig. 1, B and C, following immune cell infiltration, islets became smaller (Fig. 1B), and immune cells exhibited a trend toward increase and then decrease (although not statistically significant, Fig. 1C). The beta cell area and ratio relative to all endocrine cells were significantly higher in 5- to 9-wk-old mice compared with other age groups (Fig. 1, D and E). Therefore, we considered this age group (5–9 wk) to be the baseline control with relatively little insulitis and used mice aged 10–14 wk as having the main period of insulitis to which the other age groups were compared, when testing for statistical significance. The alpha cell area decreased upon insulitis onset and remained relatively constant at later stages, whereas
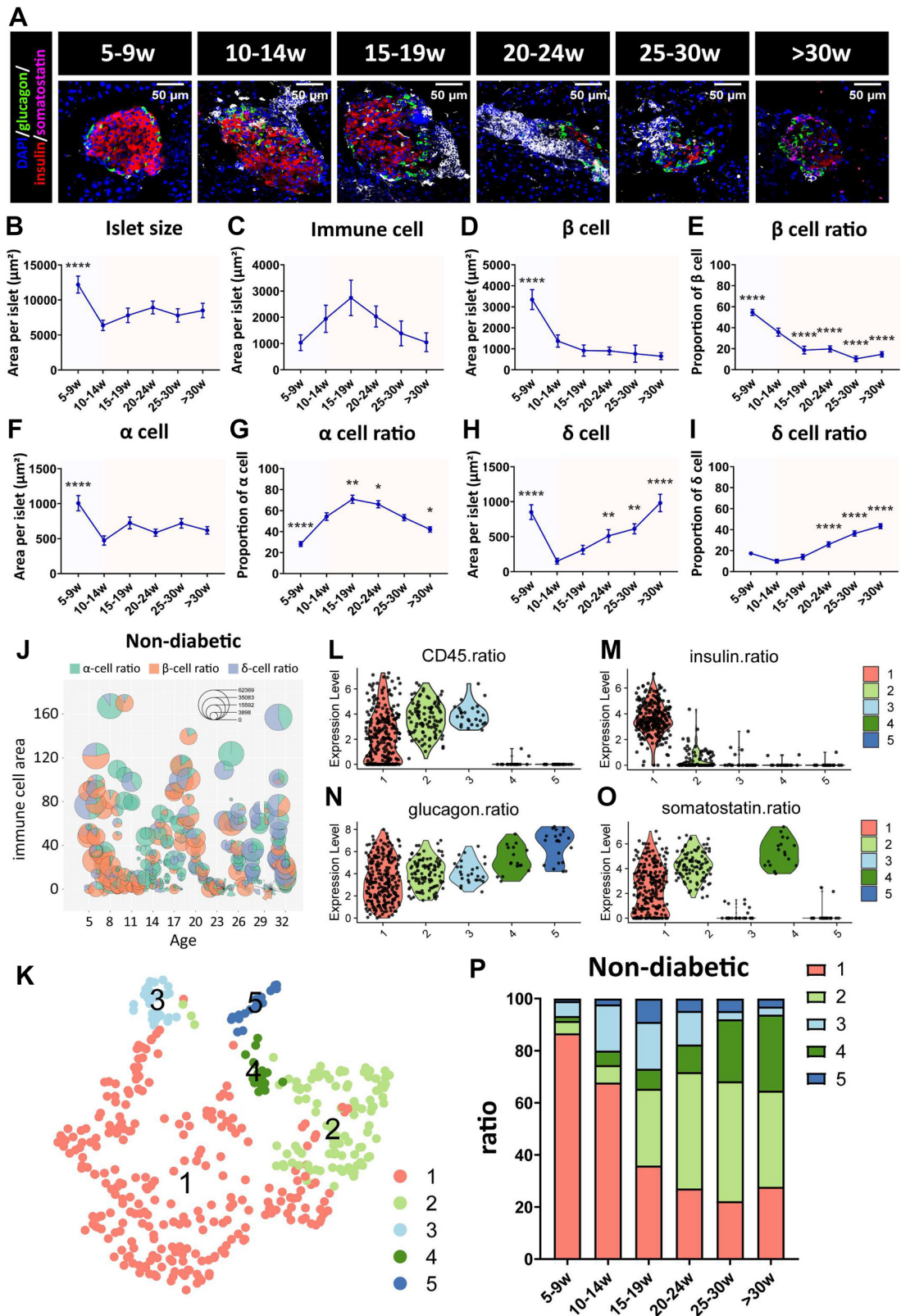
the alpha cell ratio related to all endocrine cells initially increased and then decreased (Fig. 1, *F* and *G*). Notably, from 10–14 wk to 20–24 wk, the delta cell area and ratio to all endocrine cells continued to increase after insulitis onset (Fig. 1, *H* and *I*).

A New Classification of Islet Heterogeneity Indicates an Increase in Somatostatin-Positive Islets

To further investigate changes in pancreatic islets at different ages of nondiabetic NOD mice, we analyzed islet heterogeneity in each age group, including islet size, endocrine cell proportions, and degree of infiltration. As shown in Fig. 1*J*, islets from mice of different age groups exhibited significant heterogeneity in size, number of immune cells, and endocrine cell composition. Heterogeneity was also observed within groups of mice of the same age.

To further describe this heterogeneity systematically, we used an algorithm to analyze 486 islets from 66 nondiabetic NOD mice to determine their origin. We assessed four indicators for each islet: the number of infiltrating immune cells, the proportion of three endocrine cell types, dimensionality reduction, and clustering. This resulted in five distinct subtypes (Fig. 1*K*, Supplemental Fig. S3*A*). As shown in Fig. 1, *L–O*, and Supplemental Fig. S3*B*, *cluster 1* contained only beta cells and was defined as $CD45^{+/-}Ins^{+}Gcg^{+}Sst^{+/-}$ type (including both $CD45^{+}$ and $CD45^{-}$ subtypes); *clusters 2* and *3* were heavily infiltrated by immune cells but differed in delta cell ratios, defined as $CD45^{+}Ins^{-}Gcg^{+}Sst^{+}$, and $CD45^{+}Ins^{-}Gcg^{+}Sst^{-}$ types, respectively; *clusters 4* and *5*, without immune infiltration, were defined as $CD45^{-}Ins^{-}Gcg^{+}Sst^{+}$ and $CD45^{-}Ins^{-}Gcg^{+}Sst^{-}$ types, respectively. Statistical analysis revealed that the proportion of clusters with more delta cell-positive islets (*clusters 2* and *4*, in green) increased with age, whereas the proportion of clusters with fewer delta cells in the islets (*clusters 3* and *5*, in blue) decreased (Fig. 1*P*). Combined with the earlier findings of increased delta cell area and ratio (Fig. 1, *H* and *I*), these data suggested that somatostatin-positive islets increased during autoimmunity progression in nondiabetic NOD mice.

Alpha Cells Transdifferentiate into Delta Cells in Nondiabetic NOD Mice

Given the observed increase in somatostatin-positive islets and delta cells in older nondiabetic mice (Fig. 1, *H* and *P*), we hypothesized that there might be transdifferentiation from other endocrine cells to delta cells at different ages of nondiabetic NOD mice. Intriguingly, glucagon and somatostatin double-positive cells ($alpha^{+}delta^{+}$ cells) significantly increased

in nondiabetic mice after immune infiltration (>10–14 wk), peaking in 15- to 19-wk-old mice. (Fig. 2, *A–C*). These data indicated ongoing either alpha-to-delta cell or delta-to-alpha cell conversion in some islets.

To investigate the potential direction of transdifferentiation, we reanalyzed a previously published single-cell RNA sequencing data set (GEO accession: GSE117770), which included islets from 8-, 14-, and 16-wk-old nondiabetic NOD mice (20). We reconstructed the dimensionality reduction based on t-distributed stochastic neighbor embedding (t-SNE) and divided the cells into clusters (Supplemental Fig. S4). We next isolated all alpha and delta cells from different ages for further analysis (Fig. 2*D*). Based on glucagon and somatostatin expression levels, we found more double-positive cells in 14- and 16-wk-old mice (Fig. 2*E*), consistent with our immunostaining data. In addition, alpha cells from different ages were also analyzed for their identity (Fig. 2*F*). Notably, alpha cells from 14-wk-old mice expressed high levels of delta cell marker genes, suggesting a subset of alpha cells may be undergoing transdifferentiation.

To verify our hypothesis and determine the direction of differentiation, we performed pseudotime series analysis of alpha and delta cell clusters from GSE117770 (Fig. 2*G*) and constructed a trajectory (Fig. 2, *H* and *I*). Our results showed that the trajectory comprised four branches and three decision points, dividing cells into seven states (Fig. 2*J*). Alpha cells were located near the left pole, whereas delta cells were near the right pole (Fig. 2*H*). Cells near the poles indicated mature states, whereas cells in the middle zone represented transitional states, which are relatively less well-defined (Fig. 2*H*). As shown in Fig. 2*J*, *states 3*, *4*, *5*, and *6* corresponded to mature alpha cells, and *states 1* and *7* to mature delta cells, whereas state 2 represented transitional cells. Interestingly, double-positive cells were predominantly located in *states 2* and *1*, mainly from 14- and 16-wk-old mice (Fig. 2*K*). These data indicated that transitional cells, which were double-positive, developed into delta cells, retaining glucagon. Collectively, our results suggested that a subset of alpha cells transdifferentiated into delta cells during progression of autoimmunity in nondiabetic NOD mice.

Alpha Cell Dedifferentiation Followed by Transdifferentiation into Delta Cells in Nondiabetic NOD Mice

Our foregoing data demonstrated that during insulitis development in nondiabetic NOD mice, some alpha cells became double hormone-positive cells before transforming

Figure 1. Dynamic changes and high heterogeneity in endocrine cell proportions across different ages of nondiabetic NOD mice. *A*: representative images of endocrine cells in nondiabetic NOD mice from various age groups. *Top*: the respective age groups. DAPI-stained nuclei (blue), glucagon-stained alpha cells (green), insulin-stained beta cells (red), somatostatin-stained delta cells (magenta), and CD45-stained immune cells (white) are shown. *B* and *C*: comparison of islet size (*B*) and immune cell area (*C*) across different ages. Sample sizes (mice/islets per group) were as follows: 5–9 wk (10/105), 10–14 wk (11/90), 15–19 wk (11/78), 20–24 wk (11/85), 25–30 wk (11/63), and >30 wk (12/65). *D–I*: mean areas and proportions of beta, alpha, and delta cells relative to total endocrine cells in nondiabetic mice in the same age groups as in *B* and *C*, using the same sample sizes per group. *J*: analysis of islet heterogeneity in terms of composition and quantity of alpha, beta, and delta cells at different ages, based on 66 nondiabetic NOD mice and 486 islets. The x-axis shows the age of the mice, whereas the y-axis represents the square of the immune cell area surrounding the islets. The bubbles indicate islet area, with colors representing green for alpha cells, orange for beta cells, and blue for delta cells. *K*: Uniform Manifold Approximation and Projection (UMAP) clustering of the same 486 islets, grouped into 5 islet types (*clusters 1–5*). Number of mice/islets per cluster: *cluster 1* (87/272), *cluster 2* (93/224), *cluster 3* (67/123), *cluster 4* (54/121), and *cluster 5* (34/58). *L–O*: violin plots showing the ratio of areas occupied by immune cells (*L*), beta cells (*M*), alpha cells (*N*), and delta cells (*O*) relative to the total islet area in different clusters. The colors of the clusters in the violin plots are indicated on the right. *P*: proportion of the 5 types of islets at different ages of nondiabetic mice. Data are presented as means ± SE, with significance determined by one-way ANOVA compared with the 10- to 14-wk age group, which represents the main period of insulitis in prediabetes: *$P < 0.05$; **$P < 0.01$; and ****$P < 0.0001$. NOD, nonobese diabetic.

into delta cells. To investigate whether this transdifferentiation occurred directly or involved dedifferentiation followed by transdifferentiation, we focused on neurog3 (Ngn3), a master transcription factor regulating endocrine cell differentiation and maturation, primarily expressed in endocrine precursor cells (22). We performed immunofluorescent staining on islets from nondiabetic NOD mice to detect glucagon,

somatostatin and Ngn3. As shown in Fig. 3, A and B, many Ngn3-positive alpha cells were detected at 5–9 wk, 10–14 wk, and 15–19 wk, peaking at 10–14 wk. Most Ngn3-positive cells were glucagon positive (Fig. 3A). Interestingly, the peak of Ngn3-positive cells (Fig. 3B, solid line) slightly preceded the peak of glucagon and somatostatin double-positive cells (Fig. 3B, dashed line).
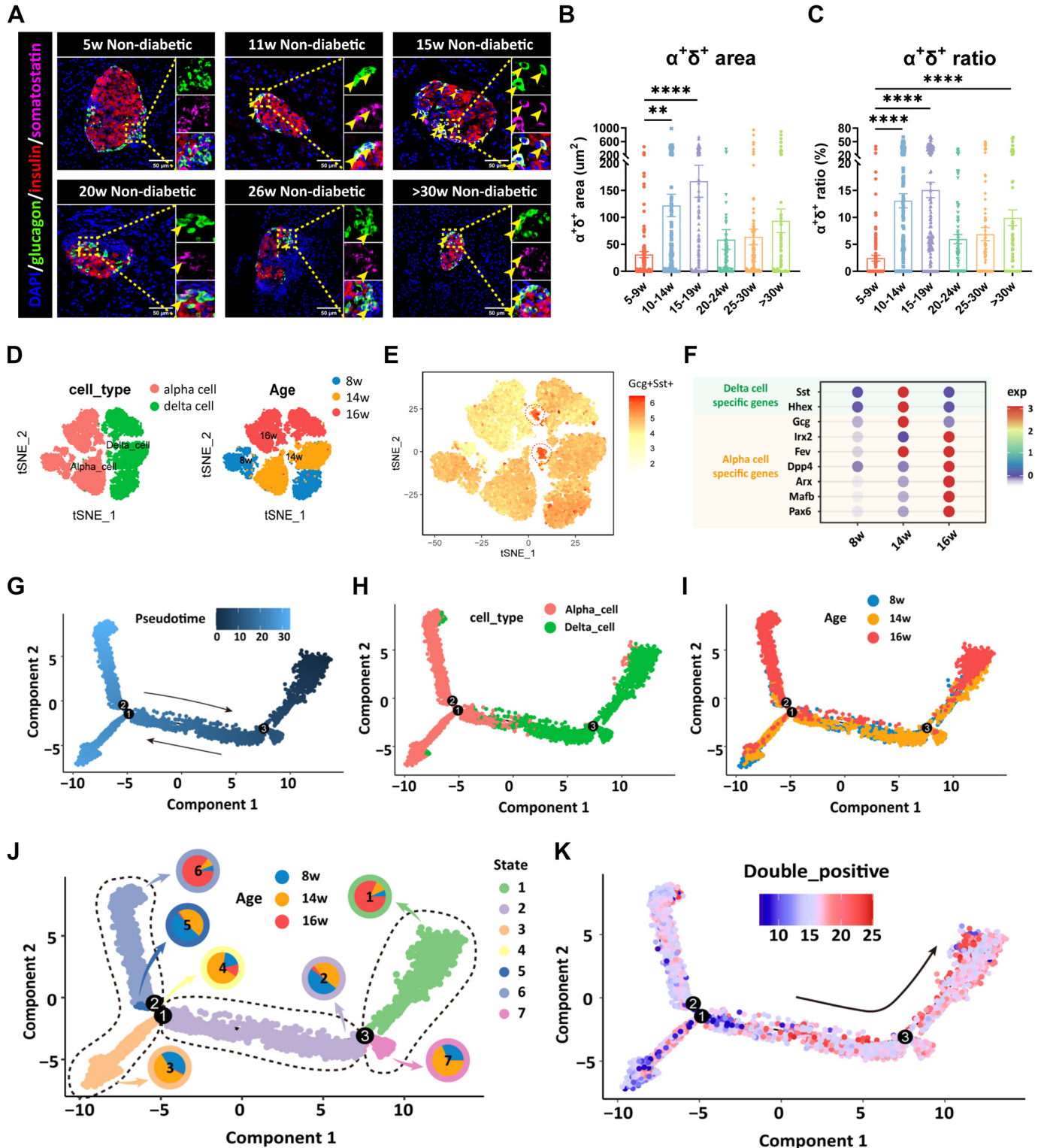
To confirm that the alpha cells in nondiabetic mice dedifferentiated and then transdifferentiated into delta cells, we performed immunostaining with another precursor and dedifferentiation marker, Sox9. As shown in Fig. 3C, many glucagon-positive cells at 13–30 wk were Sox9-positive, peaking at 13 wk. In addition, dedifferentiation marker Aldh1a3 and precursor cell marker Nkx6.1 were also found in some alpha cells at 14 wk (Supplemental Fig. S5). We also analyzed these precursor and dedifferentiation genes using the published single-cell sequencing data GSE117770 (20). As shown in Fig. 3D, Ngn3 levels in alpha cells gradually increased from 8 to 16 wk during autoimmune progression. In addition, Sox9 and Aldh1a3 levels increased at 14 wk and Nkx6.1 increased by 16 wk, consistent with our immunostaining results.

Taken together, these data suggested that alpha cells first dedifferentiated and then transdifferentiated into delta cells during immune infiltration between 14 and 19 wk.

Alpha Cell Proliferation Occurs Simultaneously with Alpha Cell Dedifferentiation

Given that the alpha cell population did not decrease and remained relatively constant after 10–14 wk of age (Fig. 1F), we then investigated whether alpha cells proliferated during progression of autoimmunity in nondiabetic NOD mice. By immunostaining for the proliferation marker Ki67, we found that delta cell proliferation rates were maintained at a low level across most age groups of nondiabetic NOD mice, both in terms of area and ratio (Fig. 3, E–G). However, delta cell proliferation increased in late stage mice, particularly in nondiabetic mice older than 30 wk (Fig. 3, F and G). In contrast, alpha cells exhibited high levels of proliferation during later insulitis (>10–14 wk), especially between 10 and 19 wk (Fig. 3, E–G). The peak periods of alpha cell proliferation coincided with the presence of glucagon and somatostatin double-positive cells (Fig. 2, A–C), indicating that alpha cell proliferation occurred simultaneously with alpha cell dedifferentiation, maintaining the alpha cell mass relatively constant in nondiabetic NOD mice.

Increased Delta Cells Suppress Glucagon Secretion in Older Nondiabetic Mice

To investigate whether the increase in delta cells affected hormone secretion from endocrine cells, we isolated islets from non-diabetic NOD mice of different ages and measured glucagon, insulin and somatostatin content (Fig. 4, A–C). As expected, glucagon levels increased with age (Fig. 4A), while insulin content in islets gradually decreased (Fig. 4B), and somatostatin content gradually increased (Fig. 4C), consistent with changes in the beta and delta cells, respectively (Fig. 1, D and H). Since somatostatin receptor 2 (Sstr2) is the primary somatostatin receptor expressed in human and mouse alpha cells (23), we cultured islets from nondiabetic NOD mice of different ages in vitro, with or without the Sstr2 inhibitor DOTA-JR11, and measured hormone secretion levels after 2 h (Supplemental Fig. S6) and 24 h (Fig. 4, D–F) of culture. Interestingly, DOTA-JR11 treatment significantly increased the glucagon secretion (Fig. 4D and Supplemental Fig. S6A), whereas there was no significant change in insulin (Fig. 4E and Supplemental Fig. S6B) or somatostatin (Fig. 4F and Supplemental Fig. S6C) secretion upon Sstr2 inhibition, indicating the inhibitory effect of somatostatin on glucagon responses. Moreover, somatostatin secretion in islets from older mice also increased with age (Fig. 4F).

Since glucagon secretion depends on cytoplasmic Ca^{2+} concentration (24), we evaluated the Ca^{2+} response of alpha cells (identified by response to adrenaline stimulation) from nondiabetic NOD mice at different ages using the Ca^{2+} indicator Fluo-4 AM (25) and recorded these with confocal microscopy time-lapse imaging (Supplemental Fig. S7). As shown in Fig. 4G, with age, the alpha cell response to low glucose gradually decreased (Fig. 4G, times between 200 and 400 s), including the response amplitude (Fig. 4H, 1 mM glucose) and response speed (Fig. 4I, 1 mM glucose). In addition, alpha cells in older (20–30 wk old) mice exhibited dysfunctional responses to adrenaline (Fig. 4G, times between 400 and 600 s). Interestingly, after Sstr2 inhibitor treatment, the oscillation amplitude of cytoplasmic Ca^{2+} concentration in alpha cells significantly increased in older mice, whereas the response was weaker in younger mice (5–14 wk old) (Fig. 4G, times between 600 and 800 s).

To investigate whether DOTA-JR11 treatment has a similar effect on glucagon secretion in vivo, we administrated 18-wk-old nondiabetic female NOD mice with DOTA-JR11. We then fasted these mice stared from 3 h after injection, then measured the glucose and glucagon levels at 6 and 12 h after injection (Fig. 4, J and K). All mice showed a gradual decrease of glucose level and an increase of glucagon level at 6 h after injection, whereas the DOTA-JR11-injected group

Figure 2. Alpha cells transdifferentiate into delta cells in nondiabetic NOD mice. A: representative images of glucagon and somatostatin double-positive endocrine cells in nondiabetic NOD mice at different ages, as indicated by the top labels. The cells within the dashed boxes are magnified in the right panel of each image. Yellow arrows indicate glucagon and somatostatin double-positive cells. DAPI-stained nuclei (blue), glucagon-stained alpha cells (green), insulin-stained beta cells (red), and somatostatin-stained delta cells (magenta) are shown. B and C: quantification of the area (B) and proportion (C) of alpha + delta double-positive cells relative to all endocrine cells at different ages. Sample sizes (mice/islets per group) were as follows: 5–9 wk (10/105), 10–14 wk (11/90), 15–19 wk (11/78), 20–24 wk (11/85), 25–30 wk (11/63), and >30 wk (12/65). D: t-SNE projection based on marker genes of alpha and delta cells and NOD mouse sources from different age groups for subsequent analysis (based on GSE117770). E: t-SNE projection of alpha and delta cells based on glucagon (gcg) and somatostatin (sst) expression levels. Scale ranges correspond to double gene (gcg and sst) expression as indicated. The red dashed line highlights cells with high expression of both gcg and sst. F: expression levels of endocrine cell markers in isolated alpha cells from different ages. Selected endocrine cell genes are indicated on the left. Scale ranges correspond to gene expression levels as indicated. G–I: pseudo-time trajectory analysis of alpha and delta cells from different ages based on pseudotime values (G), cell types (H), and ages (I). Numbers 1, 2, and 3 indicate decision points 1, 2, and 3, respectively. In G, color gradation depends on the pseudotime value ranging from 0 to 30. J: total alpha and delta cells from different ages were divided into 7 states based on pseudotime trajectory analysis. The proportion of cells from each age group in each state is shown in the pie charts. K: expression of glucagon-somatostatin (gcg-sst) double-positive cells along the pseudotime trajectory. Color indicates the expression level in each cell. Data are presented as means ± SE, with significance determined by one-way ANOVA: **$P < 0.01$; ****$P < 0.0001$. NOD, nonobese diabetic; t-SNE, t-distributed stochastic neighbor embedding.

showed significantly higher glucagon level than control group. At the 12 h, the DOTA-JR11-injected mice show higher glucose and glucagon levels compared with control group. These data may indicate that blockade of somatostatin signaling reverses alpha cell suppression in nondiabetic NOD mice in vivo.

Taken together, these results indicate that the increase in delta cells, associated with age, suppresses glucagon secretion in nondiabetic NOD mice through somatostatin production.

Alpha-to-Delta Cell Transdifferentiation Was Not Observed in Diabetic NOD Mice

To explore whether alpha-to-delta cell transdifferentiation also occurred in diabetic NOD mice, we harvested pancreata from 61 NOD mice with varying ages of diabetes onset and performed immunostaining (Supplemental Fig. S8A). There were no statistically significant differences in islet size or the number of infiltrating immune cells within different groups in diabetic mice, whereas the islet size and infiltrating
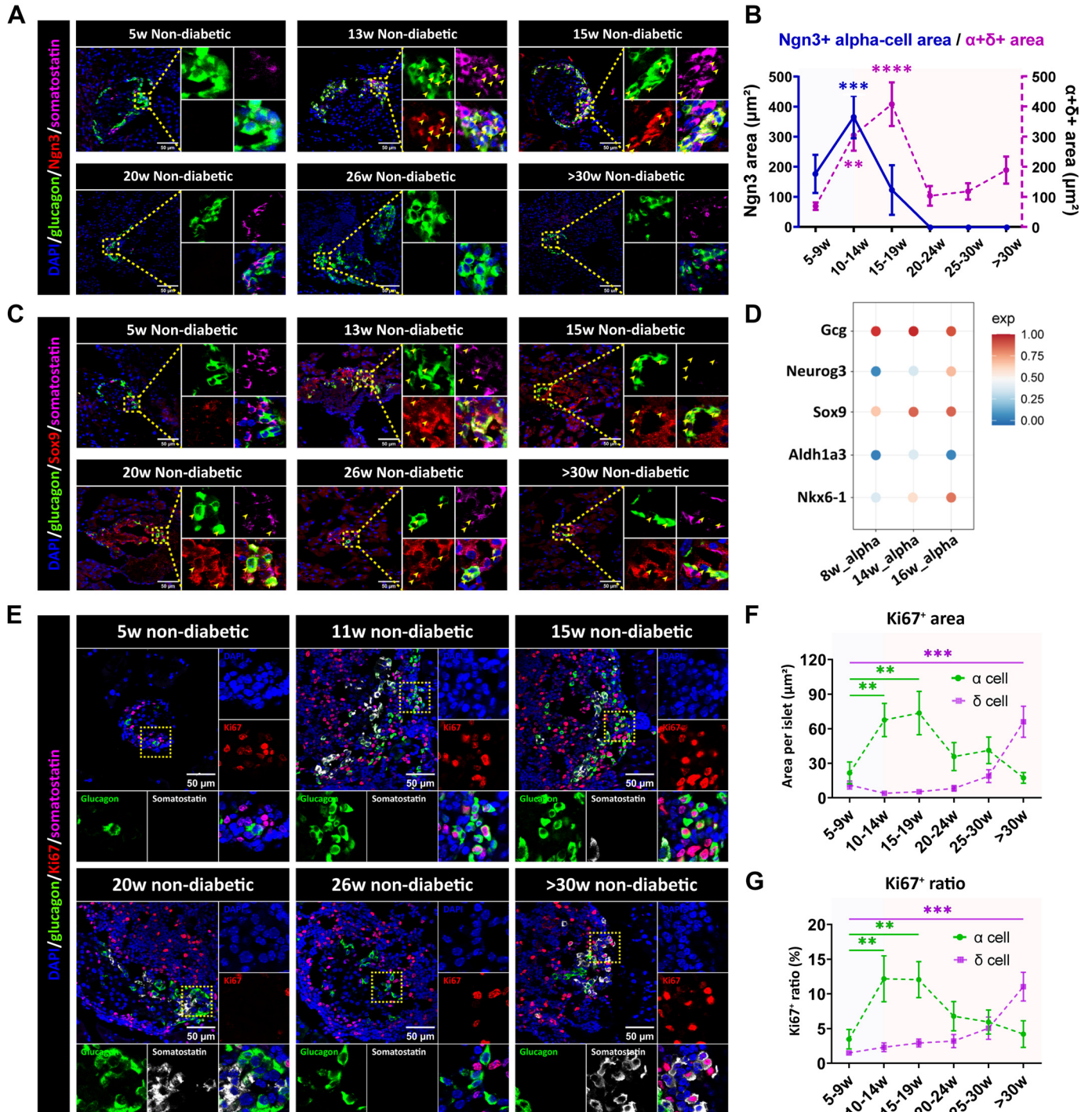
immune cells were lower than nondiabetic groups (Fig. 5, *A* and *B*). Beta cell area and ratio were very low in all diabetic mice (Fig. 5, *C* and *D*), whereas alpha cell area and ratio remained unchanged (Fig. 5, *E* and *F*). Although delta cell numbers showed a trend to increase with age in diabetic NOD mice, this was not statistically significant due to variability (Fig. 5, *G* and *H*). Moreover, the delta cell numbers were also no difference compared with same age of nondiabetic NOD mice (Fig. 5*G*). Although the ratio of delta cell in earlier stages diabetic NOD mice is higher than nondiabetic group, it is most likely due to the extremely loss of beta cells (Fig. 5*H*).

The islets in diabetic mice were also highly heterogeneous (Supplemental Fig. S8*B*). We classified the islets of diabetic mice according to the same clustering method used for nondiabetic mice (*clusters 1 to 5* as shown in Fig. 1, *L–O*). Compared with the changes in the proportion of islet clusters in nondiabetic mice of different age groups (Fig. 1*P*), the proportions of the five clusters in diabetic mice at different ages of diabetes development were similar (Fig. 5*I*).

We then stained and counted alpha$^+$ delta$^+$ double-positive cells (Supplemental Fig. S9*A*) and Ngn3-positive cells (Supplemental Fig. S9*B*) in diabetic NOD mice of all ages. The numbers of alpha$^+$ delta$^+$ double-positive cells were very low in diabetic mice (Fig. 5, *J* and *K*, and Supplemental Fig. S9*A*). Furthermore, Ngn3-positive and Sox9-positive alpha cells were barely detectable (Fig. 5*L*, Supplemental Fig. S9, *B* and *C*). Aldh1a3- or Nkx6.1-positive alpha cells were also scarcely detected in 14-wk-old diabetic NOD mice (Supplemental Fig. S10, *A* and *B*). In addition, the proliferation of alpha and delta cells in diabetic mice was much lower compared with nondiabetic mice (Fig. 5, *M* and *N*; Supplemental Fig. S11). Taken together, these data suggest that alpha-to-delta cell transdifferentiation was not observed in diabetic NOD mice.

DISCUSSION

The NOD mouse is widely used as an T1D animal model. Although they share the same genetic background, ~20% of female NOD mice do not develop diabetes. Understanding why these mice do not process to diabetes during the autoimmunity progression remains a subject of significant scientific interest. Studies have revealed that sex hormones, genetic heterogeneity, gut microbiome, regulatory T cells, and environmental factors are associated with the prevention of diabetes in NOD mice (26–28). Moreover, the nondiabetic NOD mice exhibit distinct islet characteristics compared with diabetic mice (16). However, the specific mechanisms underlying changes in pancreatic islet endocrine cells remain unclear.

In this study, we examined the composition of alpha, beta, and delta cells in islets at multiple timepoints throughout the progression of autoimmunity in the nondiabetic NOD mice. We observed that the alpha cell area remained relatively constant after immune cell infiltration (Fig. 1*F*), whereas the delta cell area significantly increased in older mice (Fig. 1*H*). There was notable heterogeneity in islet size, endocrine cell composition, and degree of infiltration (Fig. 1*J*). Although it is known that there is heterogeneity in beta cell destruction and immune cell infiltration (16, 29), our study provides a more comprehensive evaluation of islet heterogeneity, including size, composition of different endocrine cells, and immune infiltration at different ages during autoimmunity progression. Based on these observations, we proposed a new classification system, dividing islets into five subtypes (Fig. 1, *K–O*), based on the beta cell composition, immune cell infiltration, and further subdivisions according to alpha and delta cell composition, providing a more detailed description than previously published (30, 31). Using this new classification, we found an increase in somatostatin-positive islets following immune cell infiltration (Fig. 1*P*).

In 10- to 14- and 15- to 19-wk-old (established insulitis and prediabetes) nondiabetic NOD mice, we observed a significant increase in glucagon and somatostatin double-positive cells (Fig. 2, *A–C*). Furthermore, we demonstrated that these double-positive cells were undergoing transdifferentiation from alpha to delta cells (Fig. 2, *D–K*). These alpha-to-delta transdifferentiated cells first dedifferentiated into precursor cells before differentiating further into delta cells, as evidenced by increased expression of Ngn3, Sox9, Aldh1a3, and Nkx6.1 (Fig. 3, *A–D*), accompanied by simultaneous alpha cell proliferation (Fig. 3, *E–G*). The alpha cell to delta cell transdifferentiation in nondiabetic NOD mice was not due to beta cell loss, since the beta cells keep constant after 15–19 wk old in nondiabetic mice (Fig. 1*D* and Fig. 5*D*) and the replication of delta cells is pretty low at these stages (except >30-wk-old NOD mice) (Fig. 3*G*). The dedifferentiation of alpha cell may associate with the inflammatory cytokines

Figure 3. Analysis of alpha cell dedifferentiation and proliferation in nondiabetic NOD mice at different ages. *A*: representative images of endocrine cells in nondiabetic NOD mice at different ages, as indicated by the *top* labels. The dashed box is magnified in the *right* panels of each image. Yellow arrows indicate Ngn3-positive cells. DAPI-stained nuclei (blue), glucagon-stained alpha cells (green), somatostatin-stained delta cells (magenta), and Ngn3-positive cells are stained in red. *B*: quantification of Ngn3-positive area at different ages in NOD mice. The blue solid line indicates the area of alpha + Ngn3 + double-positive cells. Sample sizes (mice/islets per group) were as follows: 5–9 wk (3/21), 10–14 wk (3/17), 15–19 wk (3/16), 20–24 wk (3/15), 25–30 wk (3/14), and >30 wk (3/15). The magenta dashed line indicates the area of alpha + delta + double-positive cells. Sample sizes (mice/islets per group) were as follows: 5–9 wk (10/105), 10–14 wk (11/90), 15–19 wk (11/78), 20–24 wk (11/85), 25–30 wk (11/63), and >30 wk (12/65). *C*: representative images of endocrine cells in nondiabetic NOD mice at different ages, as indicated by the *top* labels. The dashed box is magnified in the *right* panels of each image. Yellow arrows indicate Sox9-positive cells. DAPI-stained nuclei (blue), glucagon-stained alpha cells (green), somatostatin-stained delta cells (magenta), and Sox9-positive cells are stained in red. *D*: expression levels of several marker genes in alpha cells from mice of different ages based on single-cell sequencing data (GSE117770). Scale ranges correspond to gene expression levels as indicated. *E*: representative images of Ki67-positive alpha and delta cells in nondiabetic NOD mice at different ages, as indicated by the *top* labels. The dashed box is magnified in the side panels of each image. DAPI-stained nuclei (blue), glucagon-stained alpha cells (green), somatostatin-stained delta cells (white), and Ki67-positive cells are stained in red. *F* and *G*: quantification of Ki67-positive alpha and delta cell area (*F*) and proportion (*G*) at different ages. Sample sizes (mice/islets per group) were as follows: 5–9 wk (4/44), 10–14 wk (4/42), 15–19 wk (4/46), 20–24 wk (4/41), 25–30 wk (5/40), and >30 wk (5/43). Data are presented as means ± SE, with significance determined by one-way ANOVA compared with the 5- to 9-wk age group: **$P < 0.01$; ***$P < 0.001$; ****$P < 0.0001$. NOD, nonobese diabetic.
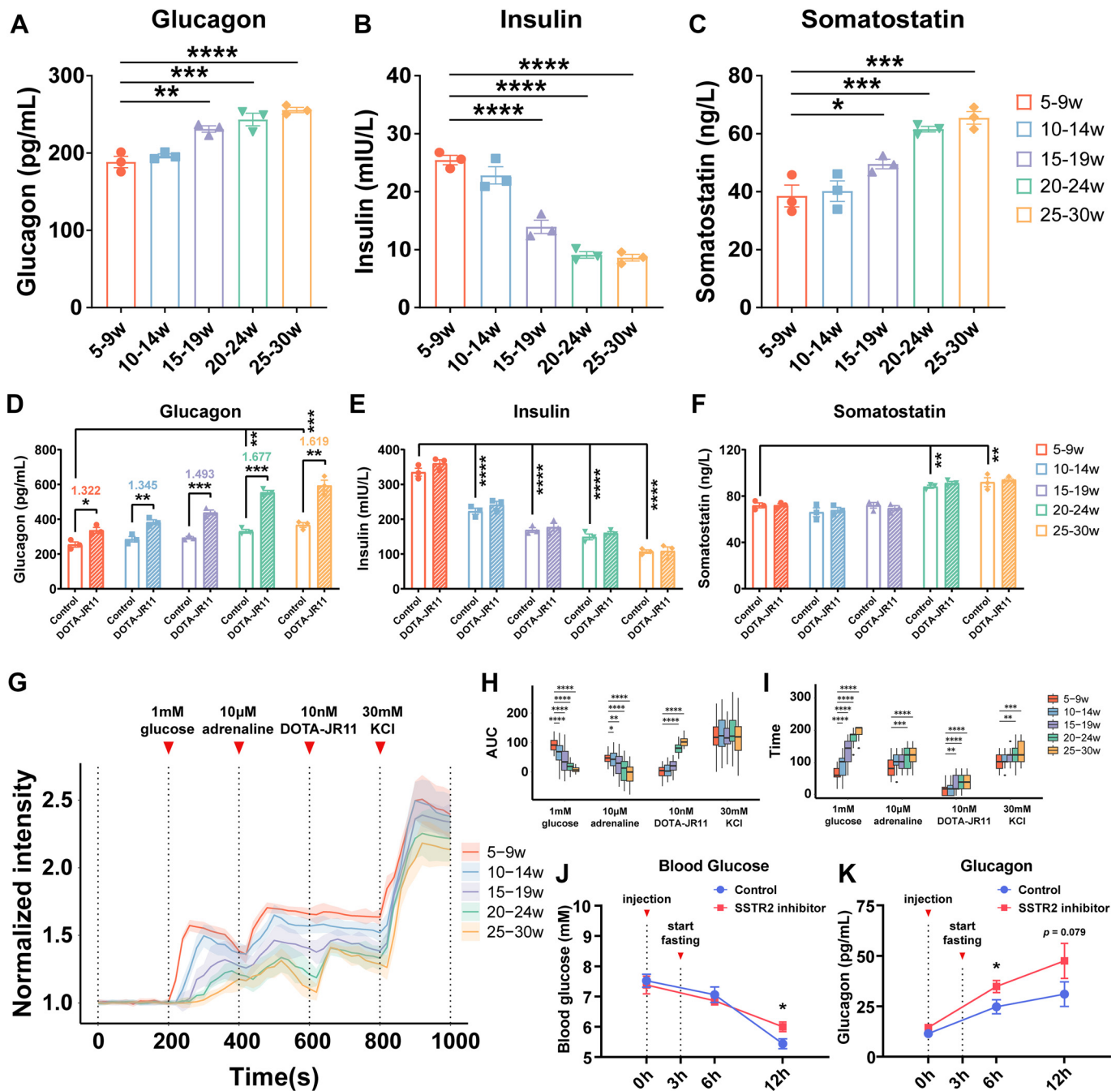
Figure 4. The increased delta cells suppress alpha cell glucagon secretion by paracrine inhibition. *A–C*: the content of glucagon (*A*), insulin (*B*), and somatostatin (*C*) in islets from nondiabetic NOD mice at different ages. Data are presented for $n = 10$ islets from $n = 3$ mice per age group. *D–F*: secretion of glucagon (*D*), insulin (*E*), and somatostatin (*F*) with and without DOTA-JR11 after culturing islets from nondiabetic NOD mice at different ages for 24 h in vitro. Data are presented for $n = 5$ islets from $n = 3$ mice. The numbers above the bars in *D* indicate the fold changes in glucagon secretion upon DOTA-JR11 treatment of islets from mice of the same age. *G*: time course of average Ca^{2+} oscillations in alpha cells in response to a series of stimulations. The calcium influx response for each alpha cell was normalized to the initial fluorescence intensity (5.5 mM glucose). Sample sizes (mice/alpha cells per group) were as follows: 5–9 wk (3/52), 10–14 wk (3/47), 15–19 wk (3/36), 20–24 wk (3/41), and 25–30 wk (3/33). *H*: area under the curve (AUC) of alpha cell responses to different stimuli from mice of different ages. *I*: time to reach peak intensity of alpha cell responses to different stimuli from mice of different ages. *J* and *K*: serial tail-tip blood sampling to monitor blood glucose (*J*) and plasma glucagon levels (*K*) in mice after SSTR2 inhibitor (DOTA-JR11) injection. Eighteen-wk-old nondiabetic NOD female mice were used, and mice started to fast from 3 h after injection. Data represent means ± SE. Statistical significance was determined by one-way ANOVA (*A–C*), Student's *t* test and 2-way ANOVA (*D–F*), and one-way ANOVA (*H* and *I*): *$P < 0.05$; **$P < 0.01$; ***$P < 0.001$; ****$P < 0.0001$. NOD, nonobese diabetic.

(IL-1β, IFN-γ, and TNF-α). Indeed, we compared the gene profiles of glucagon and somatostatin double-positive cell to the glucagon or somatostatin alone positive cell using published single-cell RNA-Seq (GSE117770), and identified that IFN-γ pathway specifically increased in the glucagon and somatostatin double-positive clusters (Supplemental Fig. S12, *A–E*). Moreover, gene set enrichment analysis (GESA) also indicated that downstream signaling cascade of IFN-γ, the Janus kinase-signal transducers and activators of transcription (JAK-STAT) pathway, was significantly enriched in double-positive cells (Supplemental Fig. S12*F*). Experimentally, we then treated αTC1-6 cells with IFN-γ. Interestingly, IFN-γ incubation significantly increased the dedifferentiation-associated genes Aldh1a3, and reduced the level of glucagon protein
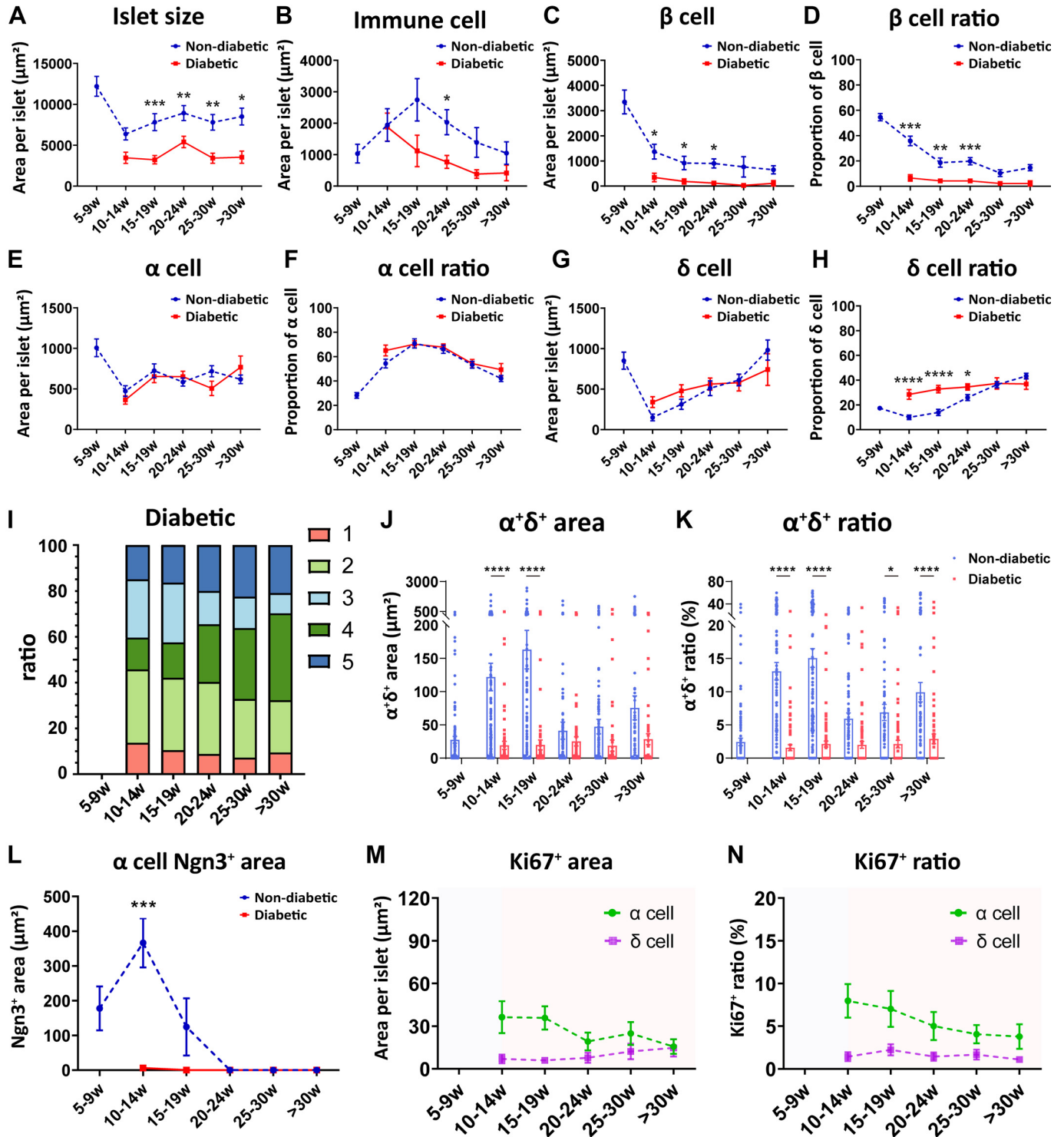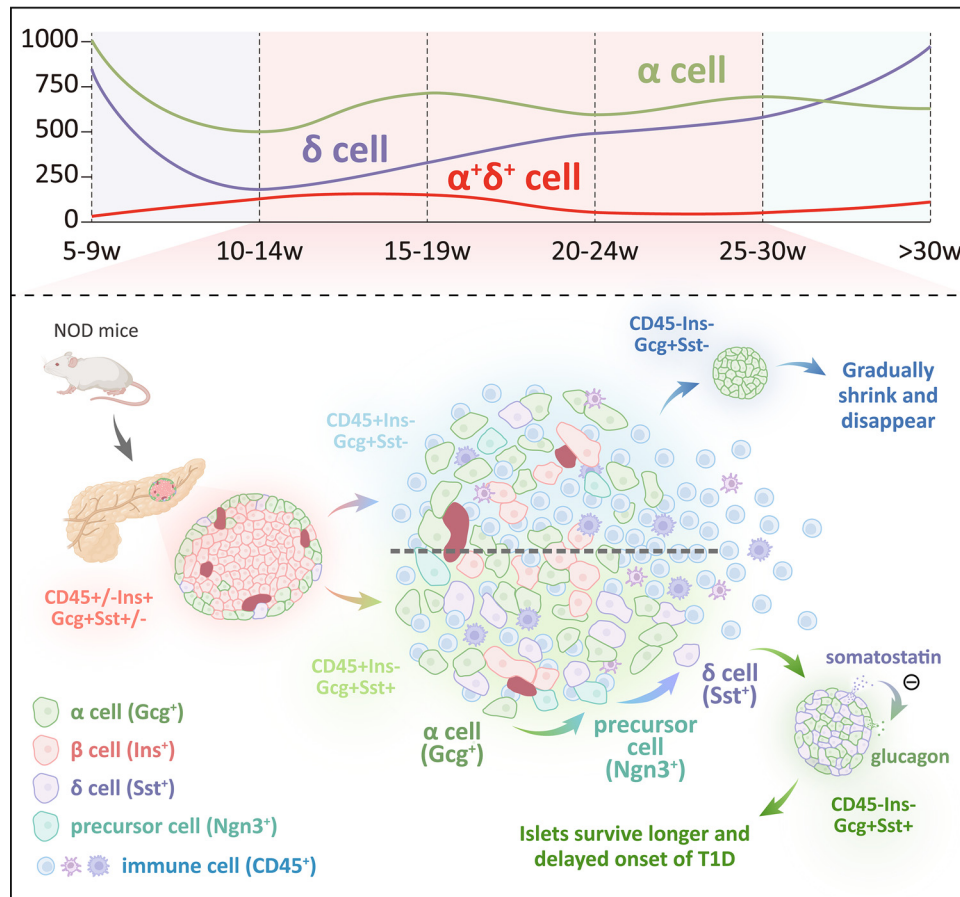
Figure 6. A working model for dynamic interactions between alpha and delta cells during autoimmune progression in nondiabetic NOD mice. Dynamic changes in alpha and delta cell areas in nondiabetic NOD mice across different age groups. The green line indicates the area of alpha cells, the purple line indicates the area of delta cells, the red line represents the area of glucagon and somatostatin double-positive cells. Before immune cell infiltration, there are sufficient beta cells (CD45$^{+/-}$Ins$^+$Gcg$^+$Sst$^{+/-}$) in the pancreas to maintain blood glucose homeostasis. As immune cells infiltrate the pancreas, beta cells are rapidly lost. Based on statistical results, 2 main types of islets emerge at this stage: one gradually transforms into islets primarily composed of alpha cells (CD45$^+$Ins$^-$Gcg$^+$Sst$^-$), whereas the other type exhibits a rapid increase in delta cell ratio (CD45$^+$Ins$^-$Gcg$^+$Sst$^+$). As beta cells continue to decrease, the number of immune cells near the islets also diminishes, and the proportion of 2 types of islets (CD45$^-$Ins$^-$Gcg$^+$Sst$^-$ and CD45$^-$Ins$^-$Gcg$^+$Sst$^+$) increases, indicating that these are the final 2 predominant forms of endocrine cell composition in the islets. Our data suggest that the increased delta cells are not primarily derived from self-proliferation but rather from the transdifferentiation of alpha cells. Some alpha cells first dedifferentiate into endocrine precursor cells (Ngn3 +) and then eventually transdifferentiate into delta cells. Moreover, the increased delta cells in the pancreas secrete more somatostatin, which inhibits glucagon secretion by alpha cells and leads to a reduced response to low glucose stimuli. NOD, nonobese diabetic.

(Supplemental Fig. S12, *G–I*). These data suggested that IFN-γ may serve as potential triggers for induction of alpha cell dedifferentiation.

However, although we observed a trend toward increased delta cells in diabetic NOD mice, we did not detect alpha-to-delta cell transdifferentiation in these mice (Fig. 5). We speculated that alpha-to-delta transdifferentiation in diabetic mice may occur before the diabetes onset based on several evidences. First, the occurrence of alpha cells to delta cells transdifferentiation was in the stages between 10- to 14-

Figure 5. Alpha to delta cell transdifferentiation was not observed in nonobese diabetic (NOD) mice. *A* and *B*: comparison of islet size (*A*) and immune cell area (*B*) in diabetic NOD mice with nondiabetic mice at different ages. Sample sizes of diabetic mice (mice/islets per group) were as follows: 10–14 wk (10/60), 15–19 wk (13/65), 20–24 wk (14/62), 25–30 wk (12/62), and >30 wk (12/63). *C–H*: quantification of beta, alpha, and delta cell areas and their proportions in diabetic NOD mice and compared with nondiabetic mice. Sample sizes per group were same as *A* and *B*. *I*: proportion of the 5 types of islets at different ages in diabetic NOD mice, classified based on Fig. 2*D*. *J* and *K*: quantification of alpha$^+$ delta$^+$ double-positive cell areas (*J*) and ratios (*K*) in NOD mice that developed diabetes at different ages and compared with nondiabetic mice. Sample sizes of diabetic mice (mice/islets per group) were as follows: 10–14 wk (10/60), 15–19 wk (13/65), 20–24 wk (14/62), 25–30 wk (12/62), and >30 wk (12/63). *L*: quantification of Ngn3-positive area in NOD mice that developed diabetes at different ages and compared with nondiabetic mice. Sample sizes (mice/islets per group) were as follows: 10–14 wk (3/12), 15–19 wk (3/13), 20–24 wk (3/13), 25–30 wk (3/11), and >30 wk (3/10). *M* and *N*: quantification of Ki67-positive alpha and delta cell areas (*M*) and ratios (*N*) in NOD mice that became diabetic at different ages. Sample sizes (mice/islets per group) were as follows: 10–14 wk (4/35), 15–19 wk (4/30), 20–24 wk (5/35), 25–30 wk (4/33), and >30 wk (5/32). Data are presented as means ± SE, with significance determined by one-way ANOVA compared with the 10- to 14-wk-old group: *$P < 0.05$; **$P < 0.01$; ***$P < 0.001$; ****$P < 0.0001$. The data of blue dash line in Fig. 5, *A–H* and Fig. 5*L* were presented in Fig. 1, *B–I* and Fig. 3*B*, and blue bar in Fig. 5, *J* and *K* were presented in Fig. 2, *B* and *C*, here just used for comparison between nondiabetic group and diabetes group.

and 15- to 19-wk-old nondiabetic mice (Fig. 2, A−C and Fig. 3, A and B), whereas the delta cell mass of these stages was slightly lower than diabetic groups, albeit there was no significant difference in delta cell mass between diabetic and nondiabetic mice (Fig. 5G). Second, the delta cell mass also kept increasing along with age at the point of they developed diabetes (Fig. 5G). Third, we did not detect the delta cell proliferation in the diabetic mice, suggesting that the increased delta cell mass was not due to delta cell proliferation (Fig. 5, M and N). The last but not the least, the nondiabetic mice we harvested earlier stages may develop to diabetes in the later stage. Taken together, based on these evidences, we propose that the increased delta cell mass in diabetic mice is a result of transdifferentiation occurred before the diabetes onset, before the stage of we harvested them. Nevertheless, the possibility that alpha-to-delta cell transdifferentiation occurs before diabetes onset cannot be excluded based on our current data. Somatostatin secreted by delta cells significantly inhibits glucagon secretion by alpha cells (32). Studies also suggested that delta cells are increased in individuals with T1D and diabetic NOD mice, exhibiting greater activation in people with T1D, which may play a protective role against hyperglycemia (33–35). Conversely, Sstr2 antagonism ameliorates insulin-induced hypoglycemia by enhancing glucagon responses (36). Our data indicate that increased delta cells and somatostatin in pancreatic islets significantly inhibit alpha cell function during autoimmunity progression in nondiabetic mice (Fig. 4). Delta cells increase as beta cells are lost, and somatostatin from these cells inhibits glucagon secretion, potentially protecting against hyperglycemia and delaying diabetes onset in NOD mice. However, increased inhibition of glucagon secretion may also lead to alpha cell dysfunction in response to low glucose.

We propose a new working model for changes within pancreatic islets during progression of autoimmunity in nondiabetic NOD mice (Fig. 6). During autoimmunity progression, immune cells infiltrate the islets, leading to a gradual of beta cell loss. Islets then undergo two distinct transition paths. In some islets, the few initial delta cells are lost along with beta cells, resulting in islets predominantly composed of alpha cells. These islets increase rapidly in younger nondiabetic mice but decrease in older mice, suggesting that this subtype gradually shrinks and eventually disappears in vivo. In contrast, another type of islet becomes more abundant in older nondiabetic mice, characterized by a significant increase in delta cell numbers as beta cells decline, and this type of islet can survive longer. This change is not age-dependent, as no significant differences in islet type proportions were observed across various age groups in diabetic mice. Although the triggers for this process remain unclear, our data suggest that the increase in delta cells is predominantly due to transdifferentiation from alpha cells, which first undergo dedifferentiation and then eventually transdifferentiate into delta cells. The increased delta cell areas in the islets contribute to higher somatostatin secretion, which inhibits glucagon release from adjacent alpha cells and mitigates hepatic glucose production, which may associate with lower glucose level in the nondiabetic NOD mice with higher delta cell mass and may have a protective role in the prevention of onset of diabetes in NOD mice.

Overall, we investigated islet heterogeneity and hormone secretion during the progression of autoimmunity in nondiabetic NOD mice. We found that not only do endocrine cell numbers and functions change but the cell composition within islets also undergoes transformation. These results enhance our understanding of the active roles played by alpha and delta cells in T1D pathophysiology and mechanisms that counteract hyperglycemia with the loss of insulin-producing beta cells. If this mechanism also occurs in humans, changes in the balance of alpha cells and delta cells may explain reduced hypoglycemic responses due to impaired glucagon counter regulation in patients receiving exogenous insulin. However, the detailed mechanism of alpha cell to delta cell transdifferentiation requires further investigation, particularly its occurrence in humans. So far, no studies reported the detection of glucagon and somatostatin double-positive cells in patients with T1D. However, studies have reported that the delta cell mass increased in patients with T1D (10). Our observation in NOD mice is consistent with human data, we only detect alpha to delta cell transdifferentiation in nondiabetic NOD mice, but not in diabetic NOD mice. Nevertheless, the alpha-to-delta cell transdifferentiation may occurs before diabetes onset in patients with T1D.

Therapeutic approaches for T1D mostly rely on insulin treatment, which may cause severe hypoglycemia due to alpha cell defects and lack of glucagon response in a subset of patients, a phenomenon recognized for many years (37). Effective management of T1D should include a focus on glucagon secretion to prevent severe hypoglycemia. Understanding the mechanisms underlying decreased glucagon secretion during T1D pathogenesis is crucial. Glucagon secretion is regulated both intrinsically (within the alpha cell itself) and in a paracrine manner (mediated by factors released by beta and/or delta cells) (38). Hence, comprehending dynamic compositional alteration of alpha, beta, and delta cells in islets during human T1D could potentially provide new therapeutic avenues.

DATA AVAILABILITY

The data generated in this study are available from the corresponding authors on reasonable request.

SUPPLEMENTAL MATERIAL

Supplemental Figs. S1–S12: https://doi.org/10.6084/m9.figshare.29959619.

ACKNOWLEDGMENTS

GRANTS

DISCLOSURES

No conflicts of interest, financial or otherwise, are declared by the authors.

AUTHOR CONTRIBUTIONS

Z.L., F.S.W., and M.L. conceived and designed research; Z.L., X.W., Q.K., Q.R., and Y.Z. (1st) performed experiments; Z.L., F.S.W., and M.L. analyzed data; Y.Z. (2nd), F.S.W., and M.L. interpreted results of experiments; Z.L. and M.L. prepared figures; Z.L. and M.L. drafted manuscript; Q.J., F.S.W., and M.L. edited and revised manuscript; M.L. approved final version of manuscript.

REFERENCES

1. **Boldison J**, **Wong FS.** Immune and pancreatic beta cell interactions in type 1 diabetes. *Trends Endocrinol Metab* 27: 856–867, 2016. doi:10.1016/j.tem.2016.08.007.

2. **Brown RJ**, **Sinaii N**, **Rother KI.** Too much glucagon, too little insulin: time course of pancreatic islet dysfunction in new-onset type 1 diabetes. *Diabetes Care* 31: 1403–1404, 2008. doi:10.2337/dc08-0575.

3. **Sherr J**, **Tsalikian E**, **Fox L**, **Buckingham B**, **Weinzimer S**, **Tamborlane WV**, **White NH**, **Arbelaez AM**, **Kollman C**, **Ruedy KJ**, **Cheng P**, **Beck RW**; **Diabetes Research in Children Network.** Evolution of abnormal plasma glucagon responses to mixed-meal feedings in youth with type 1 diabetes during the first 2 years after diagnosis. *Diabetes Care* 37: 1741–1744, 2014. doi:10.2337/dc13-2612.

4. **Raskin P**, **Unger RH.** Effect of insulin therapy on the profiles of plasma immunoreactive glucagon in juvenile-type and adult-type diabetics. *Diabetes* 27: 411–419, 1978. doi:10.2337/diab.27.4.411.

5. **Panzer JK**, **Caicedo A.** Targeting the pancreatic α-cell to prevent hypoglycemia in type 1 diabetes. *Diabetes* 70: 2721–2732, 2021. doi:10.2337/dbi20-0048.

6. **Pechhold K**, **Zhu X**, **Harrison VS**, **Lee J**, **Chakrabarty S**, **Koczwara K**, **Gavrilova O**, **Harlan DM.** Dynamic changes in pancreatic endocrine cell abundance, distribution, and function in antigen-induced and spontaneous autoimmune diabetes. *Diabetes* 58: 1175–1184, 2009. doi:10.2337/db08-0616.

7. **Plesner A**, **Ten Holder JT**, **Verchere CB.** Islet remodeling in female mice with spontaneous autoimmune and streptozotocin-induced diabetes. *PLoS One* 9: e102843, 2014. doi:10.1371/journal.pone.0102843.

8. **Novikova L**, **Smirnova IV**, **Rawal S**, **Dotson AL**, **Benedict SH**, **Stehno-Bittel L.** Variations in rodent models of type 1 diabetes: islet morphology. *J Diabetes Res* 2013: 965832, 2013. doi:10.1155/2013/965832.

9. **Kornete M**, **Beauchemin H**, **Polychronakos C**, **Piccirillo CA.** Pancreatic islet cell phenotype and endocrine function throughout diabetes development in non-obese diabetic mice. *Autoimmunity* 46: 259–268, 2013. doi:10.3109/08916934.2012.752462.

10. **Jeffery N**, **Richardson S**, **Chambers D**, **Morgan NG**, **Harries LW.** Cellular stressors may alter islet hormone cell proportions by moderation of alternative splicing patterns. *Hum Mol Genet* 28: 2763–2774, 2019. doi:10.1093/hmg/ddz094.

11. **Zyznar ES**, **Pietri AO**, **Harris V**, **Unger RH.** Evidence for the hormonal status of somatostatin in man. *Diabetes* 30: 883–886, 1981. doi:10.2337/diab.30.10.883.

12. **Hill TG**, **Gao R**, **Benrick A**, **Kothegala L**, **Rorsman N**, **Santos C**, **Acreman S**, **Briant LJ**, **Dou H**, **Gandasi NR**, **Guida C**, **Haythorne E**, **Wallace M**, **Knudsen JG**, **Miranda C**, **Tolo J**, **Clark A**, **Davison L**, **Storling J**, **Tarasov A**, **Ashcroft FM**, **Rorsman P**, **Zhang Q.** Loss of electrical beta-cell to delta-cell coupling underlies impaired hypoglycaemia-induced glucagon secretion in type-1 diabetes. *Nat Metab* 6: 2070–2081, 2024. doi:10.1038/s42255-024-01139-z.

13. **Pearson JA**, **Wong FS**, **Wen L.** The importance of the Non Obese Diabetic (NOD) mouse model in autoimmune diabetes. *J Autoimmun* 66: 76–88, 2016. doi:10.1016/j.jaut.2015.08.019.

14. **Atkinson MA**, **Leiter EH.** The NOD mouse model of type 1 diabetes: as good as it gets? *Nat Med* 5: 601–604, 1999. doi:10.1038/9442.

15. **Ferris ST**, **Carrero JA**, **Unanue ER.** Antigen presentation events during the initiation of autoimmune diabetes in the NOD mouse. *J Autoimmun* 71: 19–25, 2016. doi:10.1016/j.jaut.2016.03.007.

16. **Boldison J**, **Thayer TC**, **Davies J**, **Wong FS.** Natural protection from type 1 diabetes in nod mice is characterized by a unique pancreatic islet phenotype. *Diabetes* 70: 955–965, 2021. doi:10.2337/db20-0945.

17. **Kang Q**, **Jia J**, **Dean ED**, **Yuan H**, **Dai C**, **Li Z**, **Jiang F**, **Zhang XK**, **Powers AC**, **Chen W**, **Li M.** ErbB3 is required for hyperaminoacidemia-induced pancreatic alpha cell hyperplasia. *J Biol Chem* 300: 107499, 2024. doi:10.1016/j.jbc.2024.107499.

18. **Yuan H**, **Kang Q**, **Li Z**, **Bai X**, **Jia J**, **Han D**, **Wu X**, **Li M.** Crispr-Cas9 mediated complete deletion of glucagon receptor in mice display hyperglucagonemia and alpha-cell hyperplasia. *Biochem Biophys Res Commun* 643: 121–128, 2023. doi:10.1016/j.bbrc.2022.12.079.

19. **Jia J**, **Bai X**, **Kang Q**, **Jiang F**, **Wong FS**, **Jin Q**, **Li M.** Blockade of glucagon receptor induces alpha-cell hypersecretion by hyperaminoacidemia in mice. *Nat Commun* 16: 2473, 2025. doi:10.1038/s41467-025-57786-7.

20. **Thompson PJ**, **Shah A**, **Ntranos V**, **Van Gool F**, **Atkinson M**, **Bhushan A.** Targeted elimination of senescent beta cells prevents type 1 diabetes. *Cell Metab* 29: 1045–1060 e1010, 2019. doi:10.1016/j.cmet.2019.01.021.

21. **Trapnell C**, **Cacchiarelli D**, **Grimsby J**, **Pokharel P**, **Li S**, **Morse M**, **Lennon NJ**, **Livak KJ**, **Mikkelsen TS**, **Rinn JL.** The dynamics and regulators of cell fate decisions are revealed by pseudotemporal ordering of single cells. *Nat Biotechnol* 32: 381–386, 2014. doi:10.1038/nbt.2859.

22. **Rukstalis JM**, **Habener JF.** Neurogenin3: a master regulator of pancreatic islet differentiation and regeneration. *Islets* 1: 177–184, 2009. doi:10.4161/isl.1.3.9877.

23. **Blodgett DM**, **Nowosielska A**, **Afik S**, **Pechhold S**, **Cura AJ**, **Kennedy NJ**, **Kim S**, **Kucukural A**, **Davis RJ**, **Kent SC**, **Greiner DL**, **Garber MG**, **Harlan DM**, **diIorio P.** Novel observations from next-generation RNA sequencing of highly purified human adult and fetal islet cell subsets. *Diabetes* 64: 3172–3181, 2015. doi:10.2337/db15-0039.

24. **Tengholm A**, **Gylfe E.** cAMP signalling in insulin and glucagon secretion. *Diabetes Obes Metab* 19, 1: 42–53, 2017. doi:10.1111/dom.12993.

25. **Liew LC**, **Poh BM**, **An O**, **Ho BX**, **Lim CYY**, **Pang JKS**, **Beh LY**, **Yang HH**, **Soh BS.** JAK2 as a surface marker for enrichment of human pluripotent stem cells-derived ventricular cardiomyocytes. *Stem Cell Res Ther* 14: 367, 2023. doi:10.1186/s13287-023-03610-2.

26. **Marino E**, **Richards JL**, **McLeod KH**, **Stanley D**, **Yap YA**, **Knight J**, **McKenzie C**, **Kranich J**, **Oliveira AC**, **Rossello FJ**, **Krishnamurthy B**, **Nefzger CM**, **Macia L**, **Thorburn A**, **Baxter AG**, **Morahan G**, **Wong LH**, **Polo JM**, **Moore RJ**, **Lockett TJ**, **Clarke JM**, **Topping DL**, **Harrison LC**, **Mackay CR.** Gut microbial metabolites limit the frequency of autoimmune T cells and protect against type 1 diabetes. *Nat Immunol* 18: 552–562, 2017 [Erratum in *Nat Immunol* 18: 951, 2017]. doi:10.1038/ni.3713.

27. **Wen L**, **Ley RE**, **Volchkov PY**, **Stranges PB**, **Avanesyan L**, **Stonebraker AC**, **Hu C**, **Wong FS**, **Szot GL**, **Bluestone JA**, **Gordon JI**, **Chervonsky AV.** Innate immunity and intestinal microbiota in the development of type 1 diabetes. *Nature* 455: 1109–1113, 2008. doi:10.1038/nature07336.

28. **Lee J**, **Yurkovetskiy LA**, **Reiman D**, **Frommer L**, **Strong Z**, **Chang A**, **Kahaly GJ**, **Khan AA**, **Chervonsky AV.** Androgens contribute to sex bias of autoimmunity in mice by T cell-intrinsic regulation of Ptpn22 phosphatase expression. *Nat Commun* 15: 7688, 2024. doi:10.1038/s41467-024-51869-7.

29. **Ilonen J**, **Lempainen J**, **Veijola R.** The heterogeneous pathogenesis of type 1 diabetes mellitus. *Nat Rev Endocrinol* 15: 635–650, 2019. doi:10.1038/s41574-019-0254-y.

30. **Catrina AM**, **Popa MA**, **Văcaru AM**, **Fenyo IM.** Inflammatory status of the pancreas in NOD mice that do not develop overt diabetes. *Rom J Morphol Embryol* 62: 109–115, 2021. doi:10.47162/RJME.62.1.10.

31. **Benkahla MA**, **Sabouri S**, **Kiosses WB**, **Rajendran S**, **Quesada-Masachs E**, **von Herrath MG.** HLA class I hyper-expression unmasks beta cells but not alpha cells to the immune system in pre-diabetes. *J Autoimmun* 119: 102628, 2021. doi:10.1016/j.jaut.2021.102628.

32. **Gao R**, **Yang T**, **Zhang Q.** δ-Cells: the neighborhood watch in the islet community. *Biology (Basel)* 10: 74, 2021. doi:10.3390/biology10020074.

33. **Miranda C**, **Begum M**, **Vergari E**, **Briant LJB.** Gap junction coupling and islet delta-cell function in health and disease. *Peptides* 147: 170704, 2022. doi:10.1016/j.peptides.2021.170704.

34. **Piran R**, **Lee SH**, **Li CR**, **Charbono A**, **Bradley LM**, **Levine F.** Pharmacological induction of pancreatic islet cell transdifferentiation: relevance to type I diabetes. *Cell Death Dis* 5: e1357, 2014. doi:10.1038/cddis.2014.311.

35. **Reddy S**, **Chai RC**, **Rodrigues JA**, **Hsu TH**, **Robinson E.** Presence of residual beta cells and co-existing islet autoimmunity in the NOD mouse during longstanding diabetes: a combined histochemical and immunohistochemical study. *J Mol Histol* 39: 25–36, 2008. doi:10.1007/s10735-007-9122-5.

36. **Yue JT**, **Riddell MC**, **Burdett E**, **Coy DH**, **Efendic S**, **Vranic M.** Amelioration of hypoglycemia via somatostatin receptor type 2 antagonism in recurrently hypoglycemic diabetic rats. *Diabetes* 62: 2215–2222, 2013. doi:10.2337/db12-1523.

37. **Gerich JE**, **Langlois M**, **Noacco C**, **Karam JH**, **Forsham PH.** Lack of glucagon response to hypoglycemia in diabetes: evidence for an intrinsic pancreatic alpha cell defect. *Science* 182: 171–173, 1973. doi:10.1126/science.182.4108.171.

38. **Walker JN**, **Ramracheya R**, **Zhang Q**, **Johnson PR**, **Braun M**, **Rorsman P.** Regulation of glucagon secretion by glucose: paracrine, intrinsic or both? *Diabetes Obes Metab* 13, 1 *Suppl*: 95–105, 2011. doi:10.1111/j.1463-1326.2011.01450.x.